Transmission-and-Distribution Dynamic Co-simulation Framework for Distributed Energy Resource Frequency Response

Wenbo Wang, *Member, IEEE*; Xin Fang, *Senior Member, IEEE*; Hantao Cui, *Senior Member, IEEE*;
Fangxing Li, *Fellow, IEEE*; Yijing Liu, *Student Member, IEEE*; Thomas J. Overbye, *Fellow, IEEE*

Abstract— The rapid deployment of distributed energy resources (DERs) in distribution networks has brought challenges to balance the transmission system and stabilize frequency. DERs have the ability to provide frequency regulation services; however, existing frequency dynamic simulation tools—which were developed mainly for the transmission system—lack the capability to simulate distribution network dynamics with high penetration of DERs. Although electromagnetic transient simulation tools can simulate distribution network dynamics, the computation efficiency limits their use for large-scale transmission-and-distribution (T&D) co-simulation. This paper presents an efficient open-source T&D dynamic co-simulation framework for DER frequency response based on the HELICS platform and off-the-shelf T&D simulators. The challenge of synchronizing the simulation time between the transmission network and the DERs in the distribution network is through the detailed modeling of DERs in frequency dynamic models while DER power flow models are also preserved in the distribution networks; thereby, respecting local voltage constraints when dispatching DER power for frequency response. The DER frequency responses (primary and secondary) are simulated in case studies to validate the proposed framework. Lastly, the accuracy of the proposed co-simulation model is benchmarked, and a large T&D system simulation is presented to demonstrate the efficiency and effectiveness of the overall framework.

Index Terms—Distributed energy resources, transmission-and-distribution frequency dynamic co-simulation, primary and secondary frequency regulation.

I. INTRODUCTION

DISTRIBUTED energy resources (DERs) are being rapidly deployed in distribution networks, which brings new challenges to balance the power system and stabilize the system frequency [1]. The DER power outputs, if not optimally managed, can not only impact the local distribution voltage but also deteriorate the transmission system power balance and increase frequency fluctuations [2], [3]. Frequency regulation services—including primary frequency response (PFR), secondary frequency response (SFR), and tertiary frequency response—are used to maintain real-time system balance and frequency stability. DERs, equipped with advanced control strategies, have the capability to provide these services [4]–[7]. The recent Federal Energy Regulatory Commission Order 2222 [8] stipulates that electricity markets should remove all market access barriers to DERs to participate in the energy, capacity, and ancillary services markets; therefore, to better understand and use DER frequency regulation services, the frequency dynamic responses of DERs should be modeled in system dynamic simulations. Therefore, efficiently integrating DER dynamics into transmission system frequency dynamic simulations attracts increasing research attention. The power output of DERs hosted mainly in distribution networks may impact the local voltage profiles especially when the

penetration of DERs is high. Therefore, when using DERs providing frequency regulation services, the local voltage should also be considered to avoid over/under voltage issues in distribution networks.

Existing dynamic simulation tools, such as GE PSLF, PowerWorld Simulator and Siemens PTI PSS®E [9]–[11], are developed mainly for transmission frequency dynamic analysis, where the positive-sequence model is used with balanced three-phase assumed. In these simulations, the aggregated model is usually used such as the DER_A model [12]. Distribution networks hosting DERs, however, are normally three-phase, unbalanced, and the DER power outputs for the frequency response should not violate the local voltage constraints. There exists research focusing on steady state or quasi-static analysis of T&D networks with DERs. For instance, in [13], an interfacing variables updating algorithm between the T&D systems was proposed to improve the convergence of T&D steady-state power flow co-simulation. The accuracy and computational efficiency of the three T&D coupling protocols (decoupled, loosely coupled, and tightly coupled) was evaluated in [14] for quasi-static T&D co-simulation. The coupled T&D ACOPF in [15] used a coordinated T&D structure with a heterogeneous decomposition algorithm. The simulation tools, synchronization methods and potential research topics on transmission and distribution co-simulation were reviewed in [16]. In [17], the impacts of DERs on the transmission system economic operation were investigated in an integrated grid modeling system (IGMS).

As for T&D dynamic analysis with DERs, electromagnetic transient (EMT) simulation tools can simulate both T&D network dynamics; however, the full EMT simulation for T&D networks requires extensive simulation time—even for a medium-size network [18]. Authors of [19], [20] proposed to model and simulate power system electromechanical and electromagnetic transients by very large-scale integrated circuit (VLSI) to improve simulation efficiency. Using the full EMT simulation to simulate large-scale T&D networks is considered as computationally impractical. In [21], a hybrid EMT and phasor-domain simulation model was proposed to accelerate the EMT simulation for T&D networks. The EMT simulation was accelerated by switching between the detailed EMT simulation and the phasor-domain simulation. In [22], an integrated T&D system power flow and dynamic simulation (transient stability dynamics) was proposed, where the T&D systems are represented in three-sequence and three phases in detail, respectively. The Three Phase Dynamics Analyzer (TPDA) in [23] solved differential algebraic equations (DAE) for the unbalanced electromechanical transients using park transformation. Ref. [24] built three-phase unbalanced transient dynamics (electromechanical transient) and power flow model

for distribution systems/microgrids with synchronous generators. Ref. [25], focused on distribution systems, proposed a hybrid simulation tool to study the impacts of distributed photovoltaics (PVs) in distribution networks. Distributed PVs (DPVs) were modeled with EMT models to study their fast dynamics, interfacing feeder models in OpenDSS in [26]. Ref. [27] built a generic platform for T&D dynamic co-simulation in the framework for network co-simulation (FNCS), where dynamic simulations were used for both T&D systems. In [28], T&D dynamic co-simulation models with parallel and series computation scheme were compared, along with the discussion of the integration time step impact. Ref. [29] used a coupled T&D simulation to analyze the impacts of bulk power system faults on distribution generation response. To summarize the different T&D co-simulation models, their transmission/distribution simulators and the tested transmission/distribution networks are listed in Table 1.

There is a lack of T&D dynamic co-simulation research that focus on modeling DER frequency regulation including primary frequency regulation (PFR), secondary frequency regulation (SFR), and local voltage constraints efficiently in large-scale T&D systems. For instance, DERs provide frequency regulation by adjusting their active power outputs, but DERs might be required by local distribution operators to adjust power to maintain certain voltage ranges. The overall dynamic interaction between T&D networks with DERs dynamic response is still unknown.

To account for DER frequency regulation response in T&D

networks, this paper proposes an efficient open-source T&D dynamic co-simulation framework, where the well-established open-source T&D simulation tools are also leveraged: the high-performance transmission dynamic simulation tool ANDES [30] and the distribution network solver OpenDSS [26]. The co-simulation platform is built with the Hierarchical Engine for Large-scale Infrastructure Co-Simulation (HELICS) [31]–[33] to establish the co-simulation flow between transmission dynamic simulation and distribution quasi-static time-series (QSTS) power flow simulation. To synchronize the DER frequency response hosted by distribution networks with the transmission network, DERs are modeled with a detailed model with frequency dynamics in ANDES. The DER power outputs from the time domain simulation (TDS) are exchanged with the distribution power flow simulators through HELICS. Consequently, the DER frequency dynamic responses are considered in both the transmission frequency dynamic simulation and the distribution network power flow simulation with multiple time resolutions. Built on this architecture, along with the efficient subsystem simulators, the proposed T&D dynamic co-simulation framework is computationally efficient. As shown in Table 1, to the best of our knowledge, the proposed framework is the first of its kind T&D dynamic co-simulation model that have been tested at scale with a 2000-bus transmission network – ACTIVSg2000 [34], and distribution networks with over 1 million nodes.

Table 1. Comparison of different T&D co-simulation models

	Model	Trans. simulator	Dist. Simulator	Trans. Network	Dist. Network
[13], [14]	Static	MATLAB	OpenDSS	IEEE 9-bus system/ IEEE-39-bus system	EPRI Ckt-24
[15]	Static	MATLAB	MATLAB	IEEE 14-bus system	IEEE 57-bus system
[17]	Static	FESTIV/ Matpower	GridLAB-D	SMUD 250-bus system	SMUD distribution feeders
[21]	Dynamic	PSCAD/EMTDC/InterPSS		IEEE 9-bus system	4-bus sub-trans. and dist.
[22]	Dynamic	Three sequence model	Three phase model	IEEE 9/39-bus systems	8-bus distribution feeder
[23]	Dynamic	Three Phase Dynamics Analyzer		IEEE 39-bus systems	Utility model
[24]	Dynamic	No Trans.	GridLAB-D	No Trans.	IEEE 123-node distribution test feeder
[25]	Dynamic	No Trans.	EMT/OpenDSS	No Trans.	IEEE 8500 node
[27]	Dynamic	Dynamic three phase model	GridLAB-D	IEEE 9-bus system	IEEE 13-node distribution feeder
[28]	Dynamic	PSAT	OpenDSS	IEEE 39-bus system	5780-node distribution system
[29]	Dynamic	PSLF	OpenDSS	WECC	Three California feeders
Proposed	Dynamic	ANDES	OpenDSS	ACTIVSg2000	Over 1 million nodes distribution networks

The main contributions of this paper are summarized as below:
1) An open-source T&D dynamic co-simulation framework is developed to study DER PFR and SFR in large-scale T&D networks.
2) A novel implementation to synchronize the transmission dynamic simulation and the distribution QSTS simulation is proposed for DER PFR and SFR.

3) The DER power intermittency and local distribution voltage constraints are considered in the PFR and SFR provision. The real-time maximum power of DERs considers both the availability uncertainty and the local voltage constraints.
4) The effectiveness and scalability of the T&D dynamic co-simulation framework are demonstrated by a set of case studies including a validation case and a 2000-bus transmission network connected with distribution

networks that have over 1 million distribution nodes.

The rest of this paper is organized as follows: Section II presents the overall T&D frequency dynamic co-simulation framework using HELICS. Section III introduces the T&D network frequency dynamic model with DERs. Section IV performs the case study to demonstrate the DER PFR and SFR. The computational performance of the proposed T&D frequency dynamic co-simulation framework is discussed as well. Section V concludes the paper.

II. TRANSMISSION-AND-DISTRIBUTION FREQUENCY DYNAMIC CO-SIMULATION FRAMEWORK

The T&D dynamic co-simulation framework developed for DER frequency dynamic response is based on the HELICS platform and off-the-shelf power system simulators. This section introduces the components of the framework and develops the interfacing requirements.

A. Brief Description of HELICS

HELICS is an open-source, cyber-physical co-simulation framework for energy systems. It is designed to integrate simulators of transmission, distribution, and communication domains to simulate regional and interconnection-scale power system behaviors. Since it exploits a generalized data exchange interface, it can include other energy sectors' simulators as well. A few key concepts of HELICS that are relevant here are introduced in the following; for more details, see [31], [32]:

- **Federates** are running simulation instances of individual subsystems, sending and receiving physical and control signals to and from other federates.
- **Brokers** maintain synchronization in the federation (i.e., many federates) and facilitate message exchange among federates.
- **Simulators** are executable—that is, they can perform some analysis functions. In this context, for example, they are the transmission simulator ANDES and the distribution simulator OpenDSS. Note that the terms *federate* and *simulator* are used interchangeably in this paper.
- **Messages** are the information passed between federates during the execution of the co-simulation. The message exchange is realized through either defining subscriptions and publications functions or dedicated federate-to-federate end point communications. Note that the filter defining the communication delay or packet drops can be included in the end point communications to simulate the cyber-physical interactions in the co-simulation.

B. T&D Co-simulation Information Exchange and Interface

The T&D simulators can execute with individual federates (e.g., separate configuration files in Python or even on multiple machines with different operating systems in various languages), the time synchronization is maintained by a HELICS broker, then the information exchange needs to be defined next.

Assume the power system is composed of transmission and distribution systems; local turbine governors that control the frequency dynamic response of turbine governors of conventional generators; DER aggregators that control

individual DER frequency response. In the co-simulation framework, the information exchange among simulators in terms of simulation time is configured as loosely coupled (i.e., one inter-time step variables exchange between simulators without intra-time step iterations) as shown in Fig. 1. The information exchanges in series such that the co-simulation is robust, and the impacts of series or parallel in formation exchange can be found in [28]. For demonstration, only one transmission and one distribution network are shown in Fig. 1. Note that the HELICS platform can coordinate multiple simulations of independent distribution networks connected to the transmission network in parallel. The time steps of the T&D simulators can be different. Their information exchange is synchronized by HELICS. The dashed arrow pointing to the right denotes the simulation time; the dashed rectangles denote the changing states (in terms of simulation time) of the T&D simulators. This is also true when both the conventional generation turbine governor simulators and the DER aggregator simulators are added.
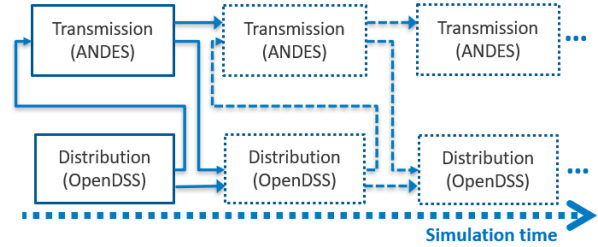

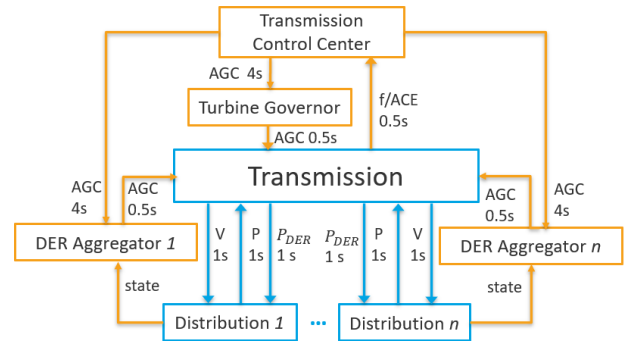Fig. 1. Simulation flow demonstration in terms of simulation time.

Fig. 2. Information exchange and time steps.

The detailed information exchanged among simulators is shown in Fig. 2, which can be seen as a snapshot of Fig. 1. The arrows denote the information exchange directions, with the exchange step time displayed which can be changed based on the simulation settings. Blue boxes and arrows represent the physical power system simulators and variables, whereas orange boxes and arrows represent the communications simulators and control signals. The transmission simulator and the distribution simulator exchange the physical variables every second including active power and voltage magnitude at the feeder heads through subscription/publication in the HELICS. The DER power is also exchanged to ensure the output of the DERs in both transmission and distribution are consistent. The transmission internal simulation time step is two cycles (33.3 milliseconds) under normal conditions. This internal step time will be reduced adaptively during the transient to improve convergence. The transmission dynamic simulator sends the

system frequency and the area control error (ACE) signals to the transmission control center through end points in the HELICS. The control center calculates the automatic generation control (AGC) signal and send it the conventional generation turbine governor and the DER aggregator every 4 seconds through end points. The turbine governors and aggregators execute their AGC through changing the power set points in their dynamic generation model in the transmission dynamic simulator every 0.5 seconds. This AGC time step can be changed based on the system settings.

In [13], the iterative coupling of the exchange variables between transmission and distribution simulators was discussed. The co-simulation model in [13] was for the steady state power flow analysis. Therefore, the iteration between T&D networks was for the same snapshot and the interfacing variables iterate between T&D until convergence. In the proposed T&D dynamic co-simulation model, the transmission simulator performs the time domain simulation (TDS) for the electromechanical dynamic analysis. Therefore, it is challenging to iterate the interfacing variables between T&D at every time step. To enable this iterative coupling in the dynamic co-simulation, the transmission dynamic simulator needs to store all intermediate state variables in the TDS which is not feasible in both the commercial dynamic simulation tools such as PSSE, PowerWorld Simulator, and PSLF and the open-source ANDES. Because intermediate state variables are usually not saved to speed up the TDS. Note that from the study in [13], it demonstrates that when the time step of the co-simulation is small, the accuracy of the loose coupling increases. In the proposed dynamic co-simulation, the time step between T&D is very small (1 second or 0.5 second). Therefore, the current non-iterative coupling between T&D can obtain highly accurate results. The accuracy of the proposed T&D dynamic co-simulation framework will be discussed in Subsection IV.A.

C. DER in QSTS Models

To match the per-unit positive-sequence equivalent calculation in the transmission simulator, the distribution system unbalanced three-phase power injection/withdraw (at the substation) are converted into the positive-sequence power injection/withdraw using the formulation (1)–(3) [35]:

$$S_i^+ = \boldsymbol{T} S_i^{abc} \tag{1}$$
$$S_i^+ = P_i^+ + j Q_i^+ \tag{2}$$
$$\boldsymbol{T} = [1/3 \quad 1/3 \quad 1/3] \tag{3}$$

where S_i^+ is the power at bus i in the transmission positive-sequence dynamic model; and $\boldsymbol{S}_i^{abc}$ is the three-phase power of the distribution network connecting the transmission bus i.

Note that the DER dynamic model is included in the transmission simulator so that the DER frequency dynamic response—both PFR and SFR—can be accurately included in the transmission frequency dynamic simulation. Most DERs are hosted in distribution systems, where local voltage needs to be maintained in the range from 0.95–1.05, along with distribution line rating limits. To account for these local requirements, the DER static power flow models are also considered in the distribution simulators. This treatment is then completed by adjusting the overall power injection/withdraw at the substation

from the distribution simulators, as in (4):

$$\boldsymbol{S}_i^{abc} = \boldsymbol{S}_{i,with\ DER}^{abc} + \sum \boldsymbol{S}_{i,DER}^{abc} \tag{4}$$

where $\boldsymbol{S}_{i,with\ DER}^{abc}$ is the distribution abc three-phase net load (the substation power), considering the DER power outputs at individual distribution nodes (the distribution feeder is connected to transmission bus i); and $\boldsymbol{S}_{i,DER}^{abc}$ is the DER power outputs in the abc three phases. $\boldsymbol{S}_i^{abc}$ is then converted to the positive sequence power using Eq. (1) and sent to the transmission simulator. Through this treatment, DER power is simultaneously modeled in both transmission and distribution networks.

D. Co-simulation Integration with HELICS

The HECLIS co-simulation platform can accommodate the aforementioned simulators of multiple time domains; the synchronization of the simulation time among different simulators is controlled implicitly by a broker, and the information exchanges are realized by either subscriptions/publications or end point communications [32]. The schematic structure is shown in Fig. 3. The HELICS command line interface (helics-cli) can be used in a Terminal script to launch the co-simulation (e.g., running all the simulators simultaneously) [32]. Note that the communications variation regarding both the latency and packets dropping can be modeled in the end points; therefore, the cyber-physical interaction can be simulated in this platform as well. The co-simulation platform includes HELICS, ANDES, and OpenDSS. All are open-source packages/software; thus, the proposed T&D frequency dynamic co-simulation platform can be used without any commercial license limitations.
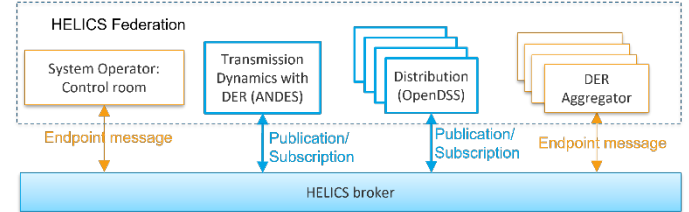
Fig. 3. Co-simulation framework structure in HELICS.

To efficiently build the co-simulation platform for large T&D systems, the platform code generation flow is described (with snippet demonstrations) as follows.

1. Read the user-defined specifications for the simulation scenarios, which can be defined in a `json` file, as shown in Listing 1.
2. Create the project directory with hierarchical subdirectories to include multiple simulation files, as demonstrated in Fig. 4.
3. Create the `json` files (shown in Listing 1) for the different simulators based on the specification information and copy them to the corresponding directories.
4. Copy the predefined simulator template files for the specific simulators (transmission dynamic simulation using ANDES and distribution power flow using OpenDSS) to the corresponding directories. The simulator template file example is shown in Listing 2.
5. Create the HECLIS `runner` file for starting up the

federation with the command line interface. The runner file example is shown in Listing 3.

Fig. 4. Project directory demonstration.

The HELICS `json` file example is shown in Listing 1 with the following remarks:
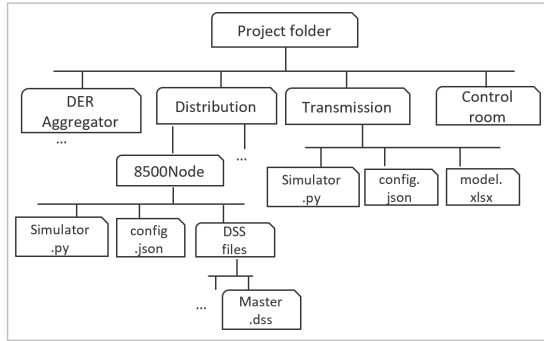
1) Line 1 and 9 declare the T&D networks.
2) Line 2 and 10 define the names of the T&D networks. IEEE 14-bus and 8500Node are the examples of T&D networks.
3) Lines 3–5 define the transmission buses and the distribution feeder mapping.
4) Lines 6–8 define the PQ load in the transmission network. Other T&D network parameters can be included in this file as well.

```
1.      {"Transmission": {
2.         "name": "IEEE14bus",
3.         "HV_MV_bus_map": {
4.            "4": "34Bus",
5.            "9": "8500Node"},
6.         "HV_PQ_index_map": {
7.            "4": "2",
8.            "9": "5"},
9.         "Distribution": {
10.           "name": "8500Node",
11.        …}
```

Listing 1. `HELICS json` file example.

The HELICS simulator template `Python` file example is shown in Listing 2:

1) Line 1 reads the simulation parameters from the specific simulator's `json` file.
2) Line 2 declares the federate execution start.
3) Line 3 defines the subscription and publication variables with other federates.
4) Line 4 loads the appropriate network data.
5) Line 5 declares the HELICS execution start.
6) Lines 6–11 define the time-based simulation with information exchange with other federates through either subscriptions/publications or end point communications.
7) Lines 12 and 13 save the simulation results and close the federate.

```
1.    Read config.json
2.    Start federate
3.    Define subscription and publication based
      on config file
4.    Load network model
5.    Start HECLIS execution mode
6.    Time based simulation:
```

```
7.       Subscribe interfacing physical variables
         from other federates
8.       Receive end point information from other
         federates
9.       Run system simulator for one time step
10.      Publish interfacing physical variables to
         other federates
11.      Send end point information to other
         federates
12.   Save results
13.   Close federate
```

Listing 2. `HELICS Simulator.py` example.

The HELICS `runner` file is shown in Listing 3:

1) Line 1 defines the HELICS broker.
2) Lines 2–12 define the federates in the HELICS co-simulation.
3) Lines 3–6 define the information of one federate (Transmission), and lines 7–10 define one distribution feeder's information. If there are multiple feeders, each feeder's information should be added here separately.
4) Line 13 defines the name of the co-simulation project.

More details about the listing example files can be found in the HELICS manual [32].

```
1.      {"broker": true,
2.         "federates": [
3.            {"directory": "./Transmission",
4.             "exec": "python -u
                  TransmissionSim.py",
5.             "host": "localhost",
6.             "name": "TransmissionSim"},
7.            {"directory":
                  "./Distribution/8500Node",
8.             "exec": "python -u 8500Node.py",
9.             "host": "localhost",
10.            "name": "8500Node"}
11.        …
12.        ],
13.        "name": "CPDS_Co-
                simulation_HELICS_Runner"
14.     }
```

Listing 3. `HELICS runner` example.

III. MODELING T&D FREQUENCY DYNAMICS WITH DERs

This section describes the T&D network dynamics with DERs respecting local voltage constraints. The dynamic model of DPV is shown in Fig. 5. More details about the parameters in this model can be found in [36]. Unlike existing models in [36], a limit for the PV's maximum available power, P_{mppt}, based on maximum power point tracking (MPPT) and other limits, is added to capture the PV's real-time total power output limitations because of the solar irradiation. Because the DPV frequency response will be constrained by its available headroom and local voltage limits. This maximum power limits should be considered. In the simulation, P_{mppt} will be a time-series input (the resolution is 1 second) based on the available DPV power output.

In Fig. 5, P_{ref} is the reference power determined in the generation scheduling model, updated every 5 minutes, which is obtained from the system operator's real-time economic dispatch. Its value is kept constant in the 5-minute interval. P_{drp} is the PFR power output from the droop response. P_{ext} is the SFR power set point, which is obtained from the system AGC control signal every 4 seconds. The total active power output of

This article has been accepted for publication in a future issue of this journal, but has not been fully edited. Content may change prior to final publication. Citation information: DOI 10.1109/TSG.2021.3118292, IEEETransactions on Smart Grid

6

P_{ref}, P_{drp}, and P_{ext} should not exceed the PV's maximum available power, P_{mppt}. This will be introduced with more details in the following subsections. Some parameters will be introduced in the following subsections and other parameters shown in Fig. 5 are explained in [36].

Fig. 5. DPV power plant generic model.

A. DER Frequency Response Modeling

1) Droop Control for PFR

The dynamic model of DPV shown in Fig. 5 includes the droop control for PFR. When the frequency drops larger than the PFR deadband, DPV will change its active power output accordingly. An additional power output, P_{drp}, will be included for its PFR:

$$P_{drp} = \begin{cases} \frac{(f_0 - db_{UF}) - f}{60} D_{dn}, f < f_0 \\ \frac{f - (f_0 + db_{OF})}{60} D_{dn}, f > f_0 \end{cases} \quad (5)$$

Where f_0 is the reference frequency (60 Hz in North America); db_{UF} and db_{OF} are the underfrequency and overfrequency deadband; and D_{dn} is the per-unit power output change to 1 per-unit frequency change (frequency droop gain).

2) SFR through AGC

As shown in Fig. 5 and Fig. 6, SFR is enabled by an AGC model that includes two components: an area-level model that calculates the area control error (ACE) from (6) in Fig. 6 and a plant-level control model that receives the ACE signal and sets the reference power P_{ext} for each plant in Fig. 5. For simplicity, assume there is one area in the simulation and no interchange with other areas, according to the North American Electric Reliability Corporation [37], [38], ACE is defined as, with the interchange metering error ignored, i.e.:

$$ACE_{tt} = 10B(f_{reqm,tt} - f_0) \quad (6)$$

where tt is the AGC time interval index; ACE_{tt} is the ACE at the AGC interval tt; $f_{reqm,tt}$ is the measured system frequency at the AGC interval tt; f_0 is the system reference frequency (60 Hz); and B is the frequency bias in MW/0.1 Hz. A positive ACE means the system is over-generating power, whereas a negative ACE means the load is larger than the generation. In this paper, a frequency error tolerance deadband, f_{db}, is introduced to eliminate the unnecessary movement of the generation set points. A proportional integral (PI) control is applied to the

ACE signal to generate the actual control signal that will be passed on to individual generators. K_p and K_i are the coefficients of the PI controller.

Fig. 6. AGC model.

The ACE signal are updated every 4 seconds to represent their discrete nature in the field. The ACE signal is then passed on to each AGC generator considering the unit's participation factor so that the individual AGC power plant's SFR power P_{ext} is updated accordingly, as input in the DPV model in Fig. 5. The participation factor of each unit's AGC response is decided by the real-time economic dispatch through the energy and regulation reserve co-optimization, as shown in Fig. 6, β_i is the i-th unit's participation factor. Since this paper focuses on the T&D dynamic co-simulation, how to calculate this participation factor is omitted. In real operation, this participation factor is optimized in real time economic dispatch considering the renewable and load variations [39]–[42].

B. Transmission Frequency Dynamic Simulation with DERs

The transmission system frequency dynamic simulation is performed with ANDES, an open-source Python-based dynamic simulation library [43]. ANDES used a hybrid symbolic-numeric framework for the system electromechanic dynamic modeling and simulation. The system dynamics can be modeled as a set of mass-matrix DAEs [44]:

$$\dot{M}x = f(x, y, u) \quad (7)$$
$$0 = g(x, y, u) \quad (8)$$

where f, g are the differential and algebraic equations, respectively; x, y, and u are the state, algebraic variables, and inputs; and M is the mass matrix. DPV dynamic model shown in Fig. 5 is added in ANDES to simulate DPV frequency dynamics [45]. The frequency deviation and ACE from the dynamic simulation are sent to the turbine governor and DER aggregators. Other DER dynamic models such as distributed energy storage will be added in ANDES as well.

C. Distribution QSTS Power Flow Simulation with DER Headroom Estimation

The distribution system QSTS power flow simulation is performed with OpenDSS. To account for the local voltage constraints that might be incurred by DER frequency dynamic response, the DERs active power outputs are modeled in distribution systems as well. As discussed in Subsection II-C, this will ensure that the DERs respect the local constraints and also fit into the overall co-simulation framework.

For DERs to provide frequency response, at a certain time step, distribution system operators or DER aggregators submit the DER headroom to the transmission system operators. This headroom is estimated through a fast (linear) optimization scheme, as in (9)– (12). The objective function (9) maximizes the total output of DERs in a specific distribution system while respecting local constraints, including voltage and thermal

limits (11), (12), as well as an equality constraint (10) of the pre-calculated voltage-power sensitivity matrix (VSM, denoted by J_{VSM}), which can be seen as power flow equations linearized at certain system states. VSM is obtained based on the method introduced in [46], but here it focuses only on the DER nodes and active power. The VSM is obtained by perturbing power injections at the nodes that are connected with DERs, one at a time, until exhausting all the DER nodes.

$$\max(\mathbf{1}^T \boldsymbol{P}_{DERs}) \tag{9}$$
$$\text{s.t. } J_{VSM}\Delta\boldsymbol{P}_{DERs} = \Delta\boldsymbol{V} \tag{10}$$
$$\underline{\boldsymbol{V}} < \boldsymbol{V}_{base} + \Delta\boldsymbol{V} < \overline{\boldsymbol{V}} \tag{11}$$
$$\underline{\boldsymbol{I}} < \boldsymbol{I} < \overline{\boldsymbol{I}} \tag{12}$$

where $\mathbf{1}$ is a column vector with all elements being 1; $\boldsymbol{P}_{DERs}$ is a column vector with size $m \times 1$ that contains the m DER outputs; $\Delta\boldsymbol{P}_{DERs}$ represents the change in DERs active power outputs; $\Delta\boldsymbol{V}$ represents the change in voltage at all nodes (assume n nodes) in the feeder; J_{VSM} denotes the sensitivity matrix with size $n \times m$; $\boldsymbol{V}_{base}$ is the base voltage values of all nodes from the current time step; and $\boldsymbol{I}$ represents the current flow in the circuits.

The output from this optimization scheme is used to calculate the total maximum headroom by (13), then it is sent to the transmission system simulator to decide the DERs available headroom for frequency regulation:

$$P_{headroom} = max(\sum\boldsymbol{P}_{DERs}) - \sum\boldsymbol{P}_{DERs}^{Base} \tag{13}$$

where $\boldsymbol{P}_{DERs}^{Base}$ is the DER output at the current time step. The transmission system simulator then considers these limits, which are shown in (14):

$$\boldsymbol{P}_{DER} = min(P_{DER}^{PFR} + P_{DER}^{SFR} + P_{DER}^{Base}, P_{mppt}, P_{caps} \ P_{DER}^{Base} + P_{headroom}) \tag{14}$$

where P_{caps} denotes the capacity ratings for DERs; therefore, with (14), the DER frequency response will respect both the transmission dynamic response and the distribution voltage limitations. Note that the DER headroom evaluation in this subsection is performed every 10 seconds in the co-simulation to reduce the co-simulation computation burden which can be adjusted based on the system setting and preference.

IV. CASE STUDIES

To illustrate the effectiveness and efficiency of the proposed framework, three systems representing different T&D network sizes are used. First, a small validation system is assembled from the IEEE 14-bus transmission system [30] and IEEE 13-bus test feeder for benchmarking purpose. After the validation case, the proposed co-simulation connects the IEEE 14-bus transmission system with two detailed distribution feeder models. Second, the IEEE 39-bus system is tested with all 19 load buses connecting various distribution feeders. Lastly, a large system of Texas 2000-bus network [47], [48] connected with 243 distribution feeders is tested. This demonstrates the superiority of the framework in computational performance. The testing simulations are performed on a personal laptop with intel CORE i7 as the CPU in the small and mid-size case studies; the large case is performed on high-performance computer Eagle at NREL [49], i.e. 96 GB memory, 18 cores of 3.0 GHz. The Python version is 3.7.
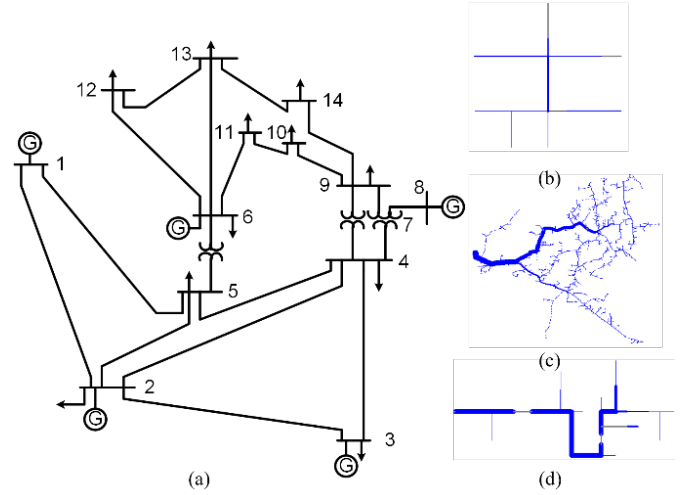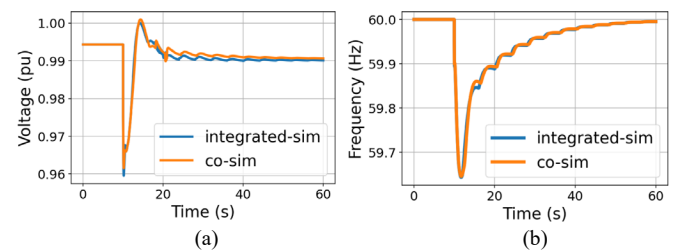

Fig. 7. Integrated T&D network with IEEE 14-bus system (a) IEEE 14-bus transmission system; (b) IEEE 13-bus feeder used for validation; (c) IEEE 8500-node feeder; and (d) IEEE 34-bus feeder.

A. IEEE 14-bus System: Validation and Co-simulation

1) Validation of the Proposed Co-simulation Framework

To validate the accuracy of the proposed T&D dynamic co-simulation framework, an integrated T&D network is created from IEEE 14-bus system and IEEE 13-bus feeder positive sequence model (converted from OpenDSS IEEE 13-bus distribution feeder original version), see Fig. 7(a) and (b). The integrated system consists of 26 buses in ANDES format (the distribution feeder head bus is Bus 11 in the IEEE 14-bus transmission network). A generation trip scenario is simulated for this integrated network, as a benchmark for comparison. Gen 3 with 40 MW power output is trip at 10 second. The same scenario is also simulated using the proposed co-simulation framework. Fig. 8 compares the voltage, frequency and DER output profiles for the two simulations. In Fig. 8, the integrated-sim means that the integrated T&D networks is simulated in ANDES. The co-sim is the case that the proposed T&D dynamic co-simulation is used for T&D networks.

It can be observed from Fig. 8 that the dynamic responses of both bulk system frequency, voltage and DER's power output from the integrated T&D network simulation and the proposed T&D dynamic co-simulation are very close. This demonstrates the accuracy of the proposed T&D dynamic co-simulation framework. The frequency and voltage profiles from the proposed co-simulation model can accurately capture the T&D network dynamics during the system transients.

This article has been accepted for publication in a future issue of this journal, but has not been fully edited. Content may change prior to final publication. Citation information: DOI 10.1109/TSG.2021.3118292, IEEETransactions on Smart Grid
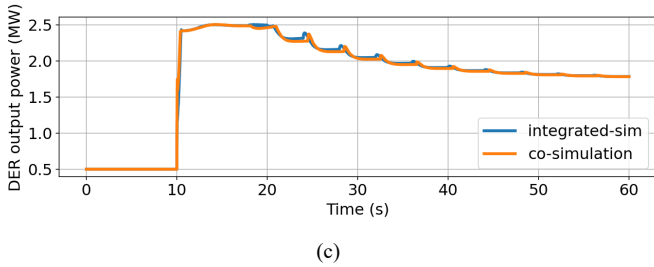
8

(c)

Fig. 8. Comparison of the integrated T&D network simulation and the proposed co-simulation: (a) voltage response; (b) system frequency response; (c) DER power output under the generation drop case.

2) Co-simulation with Two Distribution Feeders

The T&D network consists of the IEEE 14-bus system and 2 distribution feeders [50], as shown in Fig. 7(a), (c) and (d), with Bus 4 connected with the IEEE 34-bus feeder and Bus 9 connected with the IEEE 8,500-node feeder. Each feeder hosts 10 DPV units with nameplate ratings of 900 kVA. Each feeder has an aggregator coordinating the DPV AGC response in its own distribution feeder. The DPVs dispatched active power outputs are assumed 500 kW for the simulated time of 60 seconds. The transmission dynamic parameters can be found in [30]. Gen 5 in the original IEEE 14-bus system reduces its power output from 35 MW to 25 MW to accommodate the total active power output of the DERs which is 10 MW, with 0.5 MW for each DER. Here, all DERs are assumed to be DPV for simplicity; other types of DERs can be modeled as well.

3) DER AGC Response with Load Variation

This subsection studies the performance of the DPV's SFR in the proposed co-simulation model under random load variations mimicking normal operation conditions. It is assumed that loads vary randomly with a 2% standard deviation in the simulated time horizon. In this scenario, the system sends the aggregated AGC control signal to each aggregator, then the aggregators disaggregate the AGC signal to individual DERs with a 4 second interval. Because the participation factors of AGC response are normally decided by the real time economic dispatch which is not in the scope of this co-simulation model, it is assumed that 20 DPV units provide 10% of the total AGC response, with each DER providing 0.5% of the AGC response. The other conventional generation units provide 90% of the AGC response which will be evenly distributed among 5 conventional generation units.

Table 2 summarizes the statistical metrics of the system frequency and ACE. The mean frequency is close to 60 Hz. The standard deviation of frequency is small. The maximum and minimum frequency deviation is within 0.065 Hz. This shows that the T&D system frequency performance is normal under the load variation. Fig. 9 shows the system frequency and the probabilistic distribution of the frequency across the simulated time. The frequency varies mostly within a small range around +/- 0.05 Hz.

Table 2. Statistics of Frequency and ACE

Item	Frequency (Hz)	ACE (MW)
Mean	59.999	-0.172
Std	0.026	4.174
Min	59.936	-10.371
Max	60.054	8.833

Fig. 10(a) shows the DER AGC signal provided by DER

aggressors (one DER is plotted here). When the DERs do not provide SFR services, their AGC signal is zero. When the DERs provide SFR, their AGC signal will change based on the system ACE. This figure also shows that the DER AGC signal changes every 4 seconds. Fig. 10(b) further demonstrates that the output of the DER varies according to its AGC signals, where this output also considers local voltage constraints that are based on the optimization scheme in Subsection III-C and DER maximum available power (MPPT, DER capacity ratings). In this study, the DER P_{mppt} is a 1-second time-series input data (the blue dashed line). The maximum power from the VSM is calculated every 10 seconds (the green dashed line). Fig. 10(b) shows that the DER output (the orange solid line)—including its SFR response—is less than P_{mppt} (decided by irradiation) and the maximum value limited by local voltage constraints (see VSM max); therefore, both the available power variation resulting from solar radiation intermittency and the local distribution voltage limits can be respected when DERs provide SFR to the transmission system.
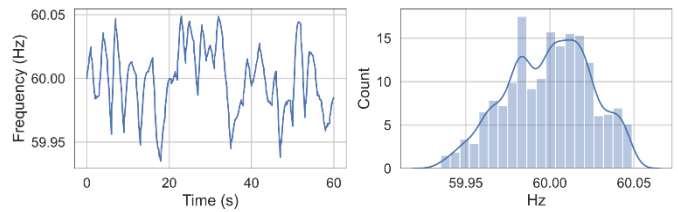

Fig. 9. System frequency and distribution.
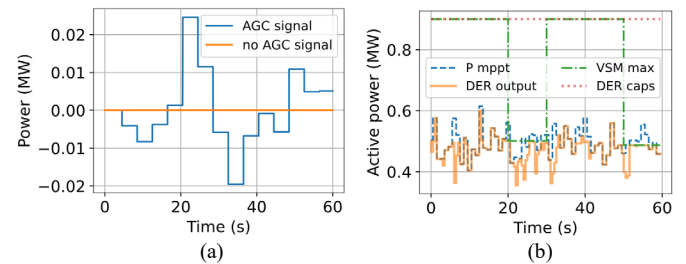

(a)   (b)

Fig. 10. (a) Example of one DER AGC signal from a DER aggregator; (b) Example of one DER power output under the load variation.

Fig. 11(a) shows the overall voltage profile for the 34-bus feeder (connected with Bus 4 of the 14-bus transmission network), and Fig. 11(b) shows the 8,500-node feeder (connected with Bus 9 of the transmission network). The blue solid line shows the average voltage within the feeder, and the shaded area denotes one standard deviation from the average. The dashed lines mark the minimum and maximum values of the feeder voltages. It can be observed that two feeders' voltages are within approximately 0.95–1.05 p.u. when the system load varies; therefore, with DERs providing SFR services, the local voltage constraints are respected using the proposed T&D frequency dynamic co-simulation model.
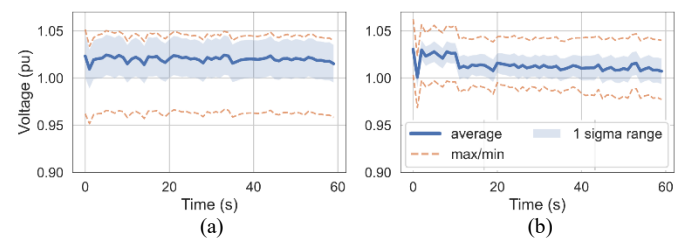

(a)   (b)

Fig. 11. Voltage plots of (a) 34-node feeder and (b) 8,500-node feeder.

4) DER PFR under Generation Outage

The DER PFR is activated when the frequency deviates more than its PFR deadband (0.017 Hz in this study) presented through a generation trip scenario here. It is assumed that Gen 3 with 40-MW power output is tripped at the fifth second. Similar to the previous subsection, 20 DERs provide 10% of the AGC response, with each DER providing 0.5% AGC response. The rest of the AGC is provided by conventional generation units. Note that the loads are kept constant in this case for clear presentation. The DER P_{mppt} varies near 0.8 MW (the blue dashed line in Fig. 12).
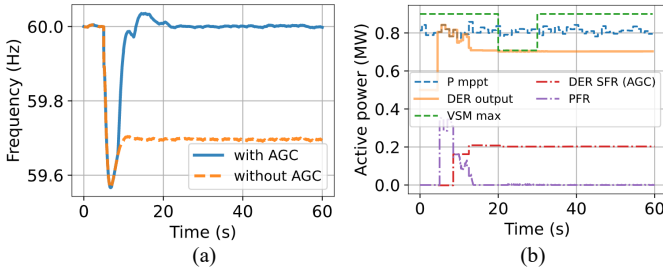
Fig. 12. (a) Frequency response with/without AGC; (b) DER power output, PFR, SFR, and its MPPT and VSM limits.

Fig. 12(a) compares the system frequency dynamic response with and without the AGC response. As expected, the frequency does not recover to 60 Hz without the AGC (SFR), although it settles at a value less than 60 Hz. With the AGC enabled, the frequency is restored to 60 Hz. Fig. 12(b) demonstrates the DER PFR and SFR after the generation outage, along with the DER actual power outputs and limits, including P_{mppt} and VSM max (the green dash line). The total power output (the orange solid line) including the reference power (i.e., the DER's dispatched power output 0.5 MW), PFR (the purple dashed line), and SFR (the red dashed line) is less than its P_{mppt} and VSM power limit; thus, these limits are respected during the DER's dynamic response. This figure also demonstrates that after the generation outage, the DER's PFR responds first by increasing DER's power output to support frequency. Then the DER's SFR starts to increase the power output to stabilize the system frequency once the DER receives the SFR signal from the aggregator. After the SFR returns the frequency to a normal level, the PFR phases out. In this simulation, the SFR signal is sent every 4 seconds thus the SFR kicks in at the eighth second as shown in the figure. Fig. 13 shows two feeders' voltage behavior in this case. After the 5th second, both feeders experience voltage dips after the generation outage, followed by small voltage overshoots that mainly result from the DER and conventional generation units' frequency responses. The fact that all these behaviors are captured shows the effectiveness and accuracy of the proposed framework.
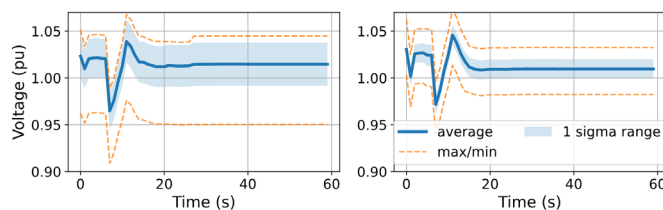

Fig. 13. Voltage response of (a) 34-bus feeder and (b) 8,500-node feeder.

B. IEEE 39-Bus System with 19 Distribution Feeders

This case study demonstrates the scalability and efficiency of the framework. In IEEE 39-bus system, all 19 loads are connected by detailed distribution feeders, as listed in Table 3. The overall T&D networks are shown in Fig. 14. Fig. 14(a) to (d) are the IEEE 39-bus transmission network, 34-bus distribution feeder, 8,500-node distribution feeder, and EPRI-J1 distribution feeder (containing 4,200 nodes). It should be noted that the original transmission active power loads do not match the original distribution feeders' active power loads, the distribution loads have to be scaled up. The scalars of individual feeders to their transmission buses are included in Table 3 as well, for the 10% DPV penetration case. These scalars might need to be tuned for different DPV penetration levels. This is because with the increasing DPV power output, the total active power at the feeder head decreases (lower power losses with a flatter voltage distance plot under a higher DPV power output).
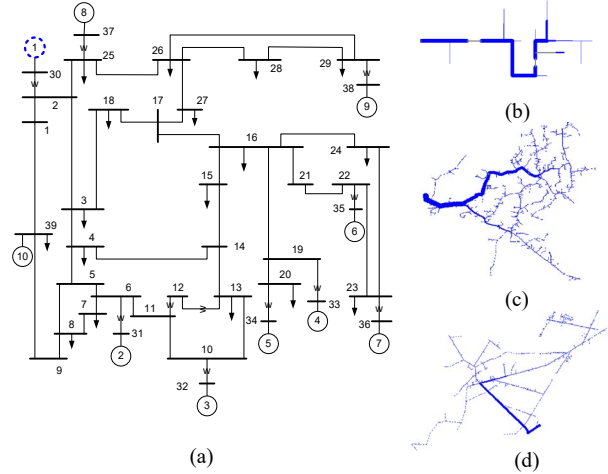

Fig. 14. The T&D system includes the (a) IEEE 39-bus transmission system with multiple feeders included: (b) 34-bus feeder, (c) 8,500-node feeder, and (d) J1 feeder.

Table 3. Transmission Bus to Feeder Mapping

T. Bus No.	D. Feeder	Scale	T. Bus No.	D. Feeder	Scale
3	34-bus	625.89	23	34-bus	258.18
4	34-bus	469.42	24	34-bus	321.92
7	34-bus	243.89	25	34-bus	233.67
8	34-bus	544.52	26	34-bus	145.00
12	8,500-node	21.19	27	34-bus	293.13
15	34-bus	333.81	28	34-bus	214.89
16	34-bus	343.61	29	34-bus	295.73
18	34-bus	164.82	31	EPRI-J1	12.69
20	8,500-node	120.05	39	34-bus	417.26
21	34-bus	285.82			

Forty DPV units are added to each distribution feeder such that there are 760 DPV units overall. Multiple scenarios with 10%–60% penetration levels of DPV in the distribution feeders are studied. Here, the penetration level is the proportion of DPV power to the system total load. The scenarios are created as follow: as the DPV penetration level increases (by increasing the power capacities and outputs of the DPVs), the generation of conventional generation units in the system reduces accordingly while keeping the total demand unchanged. For simplicity, all the conventional generation power output is reduced proportionally when the DPV penetration levels

increase. In the future, the optimal power flow model can be integrated in the co-simulation framework to consider the optimal power dispatch under specific DERs power outputs.

A generation outage (conventional generator G1 at Bus 30, as marked in Fig. 14(a) is created to demonstrate the system and DPV frequency dynamic response. It is assumed that the 760 DPV units can provide adequate AGC capacity for the system, and all the AGC (SFR) is provided by DPV units. The conventional generation units participate only in PFR provision and do not provide SFR.
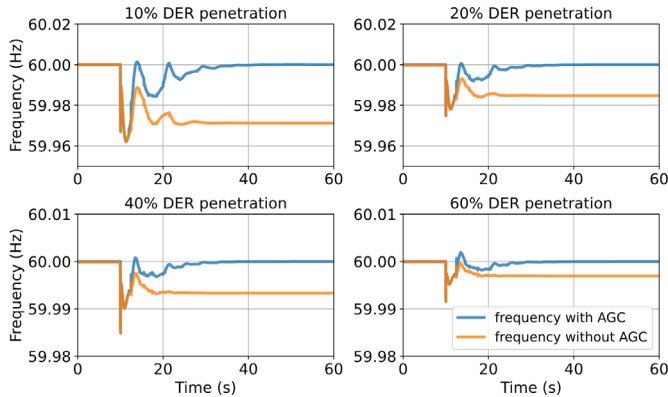
Fig. 15. System frequency response under four DER penetration levels.
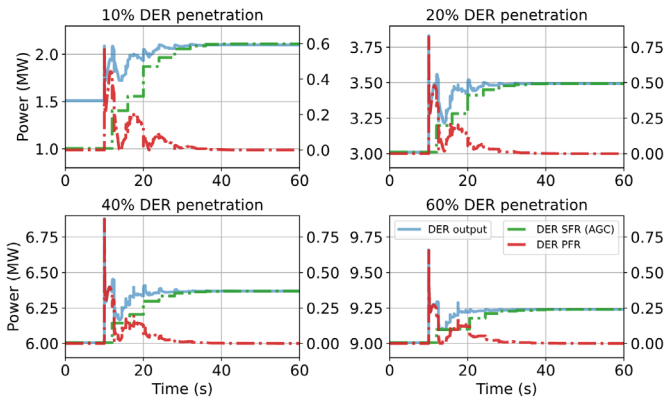
Fig. 16. DER power output, PFR, and SFR under four DER penetration levels.

Fig. 15 demonstrates the system frequency response with G1 tripped at the 10th second under various DPV penetration levels. It shows that the system frequency is restored to 60 Hz after the generation outage—this is with PFR from the conventional generation units, and PFR and SFR from the DPVs. Without DPV providing AGC, the system frequency settles to a value less than 60 Hz. Further, the frequency nadir improves with higher DPV penetration levels because the loss of the generation capacity decreases as the DPV penetration level increases.

Fig. 16 shows the DPV frequency dynamic response under four penetration levels. DPV's total power outputs (the blue solid line) are shown with the left y-axis. DPV's PFR (the red dashed line) and SFR (the green dashed line) are shown with the right y-axis. Under various penetration levels, DPV provides both PFR and SFR after the generation outage to support the transmission system frequency. Similar to the results shown in the previous subsection, PFR is activated first to increase the DPV power output. When the SFR signal is

received (at the 12th second), the SFR starts to ramp up the DPV power output and support the frequency. Meanwhile, the PFR will phase out until the frequency settles, and PFR reduces to 0. In this case, SFR signal is received at the 12th seconds and SFR starts to increase DPV power output after receiving this signal.
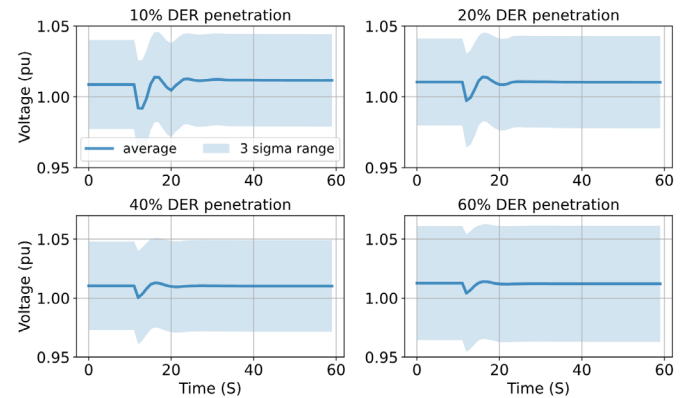

Fig. 17. Voltage profiles of 8,500-node feeder connected to Bus 20 under four DER penetration levels.

Fig. 17 shows the distribution feeder 8,500-node (connected with Bus 20) voltage profiles under four DPV penetration levels. The average voltage and the three-sigma (standard deviation) range of the voltage that covers 99% of the feeder's nodes are depicted as a solid line and a shaded area. This shows that the feeder voltages are mostly within their upper/lower limits after the generation outage under four DPV penetration levels. It can also be observed that the distribution voltage increases with DPV penetration level. With a high DPV penetration level, the feeder has a higher risk of overvoltage; therefore, the DPV sizing and location should be optimized in the distribution feeder to avoid this overvoltage issue, which is out of the scope of this paper. The proposed dynamic co-simulation model considers the local voltage limits on DERs SFR provision which can help alleviate the overvoltage issues.

C. Texas 2000-bus Co-simulation

To demonstrate the scalability the proposed T&D dynamic co-simulation model, the Texas 2000-bus synthetic transmission network is used. This system has 67 GW of load and 98GW of total generation capacity, which is built on the footprint covering most of the U.S. State of Texas [47], [48] (see Fig. 18(a)). The distribution network consist of 243 feeders, which is a subset of the Austin synthetic feeder dataset from [51], this dataset covers geographic area of Austin, Texas. (see Fig. 18(b)). These distribution feeders replace 2.83 GW of load in 39 substations in the Austin area in the transmission network. There are a total of 360k loads and 1,000,076 electrical nodes in the distribution system. There are 8400 DPVs connected to these feeders (200 DPVs at each of 36 substations and 400 DPV at each of the rest 3 substations). The total DPV power output is 222.7 MW and the total installed DPV capacity is 2.1 GW. The co-simulation is performed on a high-performance computer Eagle at NREL [49]. At the 11s, the generator at Bus 6078 with 477 MW output is tripped. The secondary frequency regulation is provided only by the connected DPVs in this system. The voltage profiles, system frequency and DER power output following this generation

This article has been accepted for publication in a future issue of this journal, but has not been fully edited. Content may change prior to final publication. Citation information: DOI 10.1109/TSG.2021.3118292, IEEETransactions on Smart Grid

11

outage event is shown in Fig. 19. Since it takes a longer time to restore the frequency to its nominal level, 160 seconds co-simulation is performed for this large system.
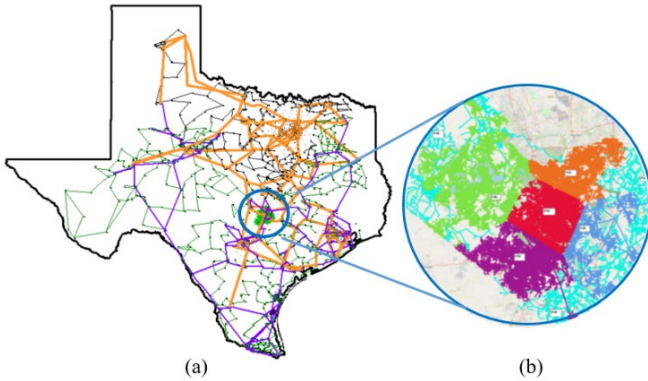

Fig. 18. (a) One-line diagram of the 2000 bus case [47] with Austin area marked green, (b) five sub-region in the distribution Austin dataset [51]
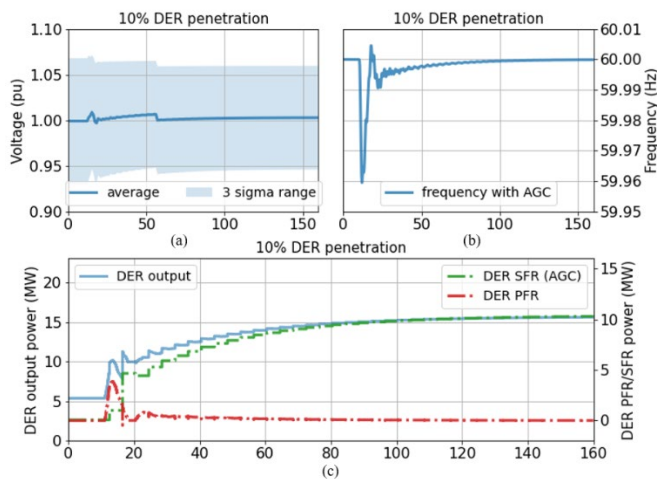
Fig. . Representative co-simulation results of the 2000-bus case (a) voltage profiles of a substation bus connected with distribution feeders (b) system frequency response (c) DER power output, PFR, and SFR.

As shown in Fig. 19, DERs provide both PFR and SFR after the generation outage. In Fig. 19(a), the local distribution voltage increases with the DERs increasing power output to support the system frequency. When the local voltage increases, the voltage regulator might be activated to reduce the voltage depending on the setting. This shows the proposed T&D dynamic co-simulation model can capture both the transmission frequency and the distribution network voltage dynamics. Fig. 19(b) shows that the system frequency drops following the generation outage, and gradually restore to the nominal value with the help of the DER PFR and SFR support (Note that the traditional generation in the system also provides PFR). DER power output is shown in Fig. 19(c), similar to the results in the previous subsections, after the contingency, PFR is activated first then, after the SFR signal is received, SFR increases DER power output and PFR gradually phases out. When the frequency is stabled, PFR reduces to 0 and SFR reaches the stable level. In this large system, it takes longer to stabilize the frequency after the contingency compared to previous smaller systems.

D. T&D Dynamic Co-simulation Computational Performance

Besides the HELICS (parallelly running separate federates),

the treatment of DER models in the proposed co-simulation framework enables the efficient and accurate simulation of DER frequency dynamic response in the large-scale T&D co-simulation environment. In the case studies, for the validation case, the integrated system simulation takes 50 seconds, whereas the co-simulation takes comparable 46 seconds on a personal laptop with Intel Core i7-10610-U processor; for the IEEE 14-bus system with 34-bus and 8,500-node T&D networks, the 60-second dynamic simulation takes approximately 60 seconds on the same machine. For the IEEE 39-bus system with 19 distribution feeders including several large-scale feeders including two 8,500-node distribution feeder, and EPRI-J1 distribution feeder (containing 4,200 nodes), the 60-second time domain T&D co-simulation takes approximately 3 minutes on the same machine. The case studies show that as the framework incorporates more detailed feeders, the computational time does not increase linearly. For the 2000-bus co-simulation, performed on HPC, the 160-second simulation takes about 48 minutes. Therefore, for the large T&D co-simulation, the proposed T&D dynamic co-simulation model can be run on HPC efficiently with relatively low cost. In terms of building the proposed co-simulation platform, an automated co-simulation model development process is designed for large-scale T&D co-simulation to set up T&D co-simulation files in the HELICS. Note that in general T&D co-simulation, it can take several seconds to synchronize all the physical variables in T&D networks at the beginning of the co-simulation. In all testing cases, the actual simulation starts after the T&D physical variables synchronized in the T&D networks in the framework.

V. CONCLUSIONS

DERs, including DPV, have been increasingly deployed in power systems. To leverage their PFR and SFR services to stabilize the system frequency, their dynamic response in T&D networks should be accurately and efficiently modeled. This paper demonstrates an efficient, open-source T&D dynamic co-simulation framework to model the frequency dynamic response of DERs providing PFR and SFR. Their impacts on both the transmission system frequency response and the distribution feeder voltage are modeled. The analyzed scenarios include normal load variation and contingencies such as generation outages. The results show that DERs can provide reliable PFR and SFR to stabilize the system frequency given certain headroom considering local voltage constraints. In addition, DPV power intermittency regarding the maximum available power and the maximum limits enforced by local distribution feeders can be endogenously considered in the proposed co-simulation model. Therefore, the real time PFR and SFR delivery can be guaranteed to maintain the transmission frequency stability and the distribution voltage profile.

The proposed framework is scalable and can greatly improves the utilization of DERs to provide grid services, which is inevitable in future power systems. Future work includes modeling all the reliability services as well as modeling more comprehensive transients and dynamic

behaviors regarding DERs power electronic devices and their controls strategies. The cyber-physical interactions such as communications latency and variations among DERs and aggregators will be investigated in the future work.

REFERENCES

[1] "NERC | Distributed Energy Resources Connection Modeling and Reliability Considerations," 2017.

[2] B. Zhang, A. Y. S. Lam, A. D. Dominguez-Garcia, and D. Tse, "An Optimal and Distributed Method for Voltage Regulation in Power Distribution Systems," *IEEE Trans. Power Syst.*, vol. 30, no. 4, pp. 1714–1726, 2015.

[3] X. Zhou, Z. Liu, C. Zhao, and L. Chen, "Accelerated Voltage Regulation in Multi-Phase Distribution Networks Based on Hierarchical Distributed Algorithm," *IEEE Trans. Power Syst.*, pp. 1–1, Oct. 2019.

[4] Z. Yi, Y. Xu, W. Gu, and Z. Fei, "Distributed Model Predictive Control Based Secondary Frequency Regulation for a Microgrid with Massive Distributed Resources," *IEEE Trans. Sustain. Energy*, pp. 1–1, 2020.

[5] M. Bayat, K. Sheshyekani, M. Hamzeh, and A. Rezazadeh, "Coordination of Distributed Energy Resources and Demand Response for Voltage and Frequency Support of MV Microgrids," *IEEE Trans. Power Syst.*, vol. PP, no. 99, pp. 1–11, 2015.

[6] Q. Shi, F. Li, G. Liu, D. Shi, Z. Yi, and Z. Wang, "Thermostatic Load Control for System Frequency Regulation Considering Daily Demand Profile and Progressive Recovery," *IEEE Trans. Smart Grid*, vol. 10, no. 6, pp. 6259–6270, Nov. 2019.

[7] X. Fang, H. Yuan, and J. Tan, "Secondary Frequency Regulation from Variable Generation through Uncertainty Decomposition: An Economic and Reliability Perspective," *IEEE Trans. Sustain. Energy*, pp. 1–1, 2021.

[8] C. Cano, "FERC Order No. 2222: A New Day for Distributed Energy Resources," 2020.

[9] "PSLF | Transmission Planning Software | GE Energy Consulting." [Online]. Available: https://www.geenergyconsulting.com/practice-area/software-products/pslf. [Accessed: 09-Dec-2020].

[10] "PSS®E – transmission planning and analysis | PSS® power system simulation and modeling software | Siemens Global." [Online]. Available: https://new.siemens.com/global/en/products/energy/energy-automation-and-smart-grid/pss-software/pss-e.html. [Accessed: 09-Dec-2020].

[11] "PowerWorld » The visual approach to electric power systems." [Online]. Available: https://www.powerworld.com/. [Accessed: 29-Jun-2021].

[12] "Reliability Guideline: Parameterization of the DER_A Model." [Online]. Available: https://www.nerc.com/comm/PC_Reliability_Guidelines_DL/Reliability_Guideline_DER_A_Parameterization.pdf. [Accessed: 24-Jun-2021].

[13] G. Krishnamoorthy and A. Dubey, "Transmission–Distribution Cosimulation: Analytical Methods for Iterative Coupling," *IEEE Syst. J.*, vol. 14, no. 2, pp. 2633–2642, Jun. 2020.

[14] R. Sadnan, G. Krishnamoorthy, and A. Dubey, "Transmission and Distribution (TD) Quasi-Static Co-Simulation: Analysis and Comparison of TD Coupling Strength," *IEEE Access*, vol. 8, pp. 124007–124019, 2020.

[15] Z. Li, Q. Guo, H. Sun, and J. Wang, "Coordinated transmission and distribution AC optimal power flow," *IEEE Trans. Smart Grid*, vol. 9, no. 2, pp. 1228–1240, 2018.

[16] S. M. Mohseni-Bonab, A. Hajebrahimi, I. Kamwa, and A. Moeini, "Transmission and distribution co-simulation: a review and propositions," *IET Generation, Transmission and Distribution*, vol. 14, no. 21. Institution of Engineering and Technology, pp. 4631–4642, 02-Nov-2020.

[17] B. Palmintier et al., "IGMS: An Integrated ISO-To-Appliance Scale Grid Modeling System," *IEEE Trans. Smart Grid*, vol. 8, no. 3, pp. 1525–1534, May 2017.

[18] A. Hariri and M. O. Faruque, "Impacts of distributed generation on power quality," in *2014 North American Power Symposium, NAPS 2014*, 2014.

[19] X. Zhang, R. Dai, P. Wei, Y. Liu, G. Liu, and Z. Wang, "Power System Transient Modeling and Simulation using Integrated Circuit," 2021.

[20] Y. Liu, X. Zhang, R. Dai, and G. Liu, "Using Terminal Circuit for Power System Electromagnetic Transient Simulation," Jul. 2021.

[21] Q. Huang and V. Vittal, "Advanced EMT and Phasor-Domain Hybrid Simulation With Simulation Mode Switching Capability for Transmission and Distribution Systems," *IEEE Trans. Power Syst.*, vol. 33, no. 6, pp. 6298–6308, Nov. 2018.

[22] Q. Huang and V. Vittal, "Integrated Transmission and Distribution System Power Flow and Dynamic Simulation Using Mixed Three-Sequence/Three-Phase Modeling," *IEEE Trans. Power Syst.*, vol. 32, no. 5, pp. 3704–3714, Sep. 2017.

[23] H. Jain, A. Parchure, R. P. Broadwater, M. Dilek, and J. Woyak, "Three-Phase Dynamic Simulation of Power Systems Using Combined Transmission and Distribution System Models," *IEEE Trans. Power Syst.*, vol. 31, no. 6, pp. 4517–4524, Nov. 2016.

[24] M. A. Elizondo, F. K. Tuffner, and K. P. Schneider, "Three-Phase Unbalanced Transient Dynamics and Powerflow for Modeling Distribution Systems With Synchronous Machines," *IEEE Trans. Power Syst.*, vol. 31, no. 1, pp. 105–115, Jan. 2016.

[25] A. Hariri and M. O. Faruque, "A Hybrid Simulation Tool for the Study of PV Integration Impacts on Distribution Networks," *IEEE Trans. Sustain. Energy*, vol. 8, no. 2, pp. 648–657, Apr. 2017.

[26] "OpenDSS / Code / [r2960] /trunk/Distrib/Doc/OpenDSSManual.pdf." [Online]. Available: https://sourceforge.net/p/electricdss/code/HEAD/tree/trunk/Distrib/Doc/OpenDSSManual.pdf. [Accessed: 09-Dec-2020].

[27] R. Huang, R. Fan, J. Daily, A. Fisher, and J. Fuller, "Open-source framework for power system transmission and distribution dynamics co-simulation," *IET Gener. Transm. Distrib.*, vol. 11, no. 12, pp. 3152–3162, Aug. 2017.

[28] R. Venkatraman, S. K. Khaitan, and V. Ajjarapu, "Dynamic Co-Simulation Methods for Combined Transmission-Distribution System with Integration Time Step Impact on Convergence," *IEEE Trans. Power Syst.*, vol. 34, no. 2, pp. 1171–1181, Mar. 2019.

[29] R. W. Kenyon, B. Mather, and B. M. Hodge, "Coupled transmission and distribution simulations to assess distributed generation response to power system faults," *Electr. Power Syst. Res.*, vol. 189, Dec. 2020.

[30] H. Cui, F. Li, and K. Tomsovic, "Hybrid Symbolic-Numeric Framework for Power System Modeling and Analysis," *IEEE Trans. Power Syst.*, pp. 1–1, Feb. 2020.

[31] B. Palmintier, D. Krishnamurthy, P. Top, S. Smith, J. Daily, and J. Fuller, "Design of the HELICS high-performance transmission-distribution-communication-market go-simulation framework," in *2017 Workshop on Modeling and Simulation of Cyber-Physical Energy Systems, MSCPES 2017 - Held as part of CPS Week, Proceedings*, 2017.

[32] "HELICS." [Online]. Available: https://helics.org/. [Accessed: 09-Dec-2020].

[33] J. Zhang et al., "Development of HELICS-based high-performance cyber-physical co-simulation framework for distributed energy resources applications," in *2020 IEEE International Conference on Communications, Control, and Computing Technologies for Smart Grids, SmartGridComm 2020*, 2020.

[34] "Electric Grid Test Case Repository." [Online]. Available: https://electricgrids.engr.tamu.edu/.

[35] J. M. T. Marinho and G. N. Taranto, "A hybrid three-phase single-phase power flow formulation," *IEEE Trans. Power Syst.*, vol. 23, no. 3, pp. 1063–1070, 2008.

[36] "WECC Distributed and Small PV Plants Generic Model (PVD1) - ESIG." [Online]. Available: https://www.esig.energy/wiki-main-page/wecc-distributed-and-small-pv-plants-generic-model-pvd1/. [Accessed: 10-Dec-2020].

[37] NERC, "Special Report: Ancillary Service and Balancing Authority Area Solutions to Integrate Variable Generation," 2011. [Online]. Available: https://www.nerc.com/files/ivgtf2-3.pdf. [Accessed: 10-May-2021].

[38] T. J. Overbye, K. S. Shetye, J. Wert, H. Li, C. Cathey, and H. Scribner, "Stability Considerations for a Synchronous Interconnection of the North American Eastern and Western Electric Grids," in *Hawaii International Conference on System Sciences (HICSS)*, 2022.

[39] X. Fang, B.-M. S. Hodge, E. Du, C. Kang, and F. F. Li, "Introducing Uncertainty Components in Locational Marginal Prices for Pricing Wind Power and Load Uncertainties," *IEEE Trans. Power Syst.*, vol. 34, no. 3, pp. 2013–2024, 2019.

[40] X. Fang, H. Cui, E. Du, F. Li, and C. Kang, "Characteristics of locational uncertainty marginal price for correlated uncertainties of variable renewable generation and demands," *Appl. Energy*, vol. 282, p. 116064, Jan. 2021.

[41] X. Fang, K. S. A. Sedzro, H. Yuan, H. Ye, and B.-M. Hodge, "Deliverable Flexible Ramping Products Considering Spatiotemporal

Correlation of Wind Generation and Demand Uncertainties," *IEEE Trans. Power Syst.*, vol. 35, no. 4, pp. 2561–2574, Dec. 2020.

[42] X. Fang, B. M. Hodge, H. Jiang, and Y. Zhang, "Decentralized wind uncertainty management: Alternating direction method of multipliers based distributionally-robust chance constrained optimal power flow," *Appl. Energy*, vol. 239, no. 2019, pp. 938–947, Apr. 2019.

[43] H. Cui and F. Li, "ANDES: A Python-Based Cyber-Physical Power System Simulation Tool," in *2018 North American Power Symposium, NAPS 2018*, 2019.

[44] H. Cui, F. Li, J. H. Chow, and L. Fellow, "Mass-Matrix Differential-Algebraic Equation Formulation for Transient Stability Simulation."

[45] "Tutorial — ANDES 1.3.0 documentation." [Online]. Available: https://docs.andes.app/en/stable/tutorial.html#interactive-usage. [Accessed: 04-Mar-2021].

[46] X. Zhu, J. Wang, N. Lu, N. Samaan, R. Huang, and X. Ke, "A Hierarchical VLSM-Based Demand Response Strategy for Coordinative Voltage Control between Transmission and Distribution Systems," *IEEE Trans. Smart Grid*, Sep. 2018.

[47] A. B. Birchfield, T. Xu, K. M. Gegner, K. S. Shetye, and T. J. Overbye, "Grid Structural Characteristics as Validation Criteria for Synthetic Networks," *IEEE Trans. Power Syst.*, vol. 32, no. 4, pp. 3258–3265, Jul. 2017.

[48] T. Xu, A. B. Birchfield, and T. J. Overbye, "Modeling, tuning, and validating system dynamics in synthetic electric grids," *IEEE Trans. Power Syst.*, vol. 33, no. 6, pp. 6501–6509, Nov. 2018.

[49] "Eagle Computing System | High-Performance Computing | NREL." [Online]. Available: https://www.nrel.gov/hpc/eagle-system.html. [Accessed: 29-Jun-2021].

[50] K. P. Schneider *et al.*, "Analytic Considerations and Design Basis for the IEEE Distribution Test Feeders," *IEEE Trans. Power Syst.*, vol. 33, no. 3, pp. 3181–3188, May 2018.

[51] N. Panossian, T. Elgindy, B. Palmintier, and D. Wallison, "Synthetic, Realistic Transmission and Distribution Co-Simulation for Voltage Control Benchmarking," *2021 IEEE Texas Power Energy Conf. TPEC 2021*, Feb. 2021.

Wenbo Wang (S'16-M'19) received the M. Sc. and the Ph.D. degrees in Electrical Engineering from Tandon School of Engineering, New York University, in 2015 and 2019. He is currently a researcher at National Renewable Energy Laboratory (NREL). His research interests include distribution system modeling and analysis, power systems stability, optimization, and data-driven methods in power systems.

Xin Fang (SM'18) received the B.S. degree from Huazhong University of Science and Technology, China, in 2009, the M.S. degree from China Electric Power Research Institute, China, in 2012, and the Ph.D. degree at the University of Tennessee (UTK), Knoxville, TN, USA, in 2016.

He is currently a senior researcher at National Renewable Energy Laboratory (NREL). Before joining NREL, he was a power system engineer at GE Grid Solutions afrom 2016 to 2017. Dr. Fang is an Associate Editor of *IEEE Transactions on Power Systems*. His research interests include power system planning and optimization, electricity market operation considering renewable energy integration, and cyber-physical transmission and distribution modeling and simulation.

Hantao Cui (SM'20) received the B.S. and M.S. degrees from Southeast University, China, and the Ph.D. degree from the University of Tennessee, Knoxville. He is an assistant professor at the School of Electrical and Computer Engineering, Oklahoma State University. He was a research assistant professor with CURENT and the Department of Electrical Engineering and Computer Science, University of Tennessee, Knoxville, from 2019 to 2021. His research interests include power system

modeling, simulation, and high-performance computing.

Fangxing (Fran) Li (F'17) received the B.S.E.E. and M.S.E.E. degrees from Southeast University, Nanjing, China, in 1994 and 1997, respectively, and the Ph.D. degree from Virginia Tech, Blacksburg, VA, USA, in 2001. He is currently the James McConnell Professor with the University of Tennessee, Knoxville, TN, USA.

His research interests include deep learning in power systems, renewable energy integration, demand response, power market and power system computing. Since 2020, he has been the Editor-In-Chief for the *IEEE Open Access Journal of Power and Energy*.

Yijing Liu (S'17) received her B.S. degree in 2017 from University of Electronic Science and Technology of China, Chengdu, P.R.C.. She is now a Ph.D. candidate in Electrical and Computer Engineering at Texas A&M University, College Station, Texas, USA. Her research interests include power system dynamics modeling, renewable resources modeling and grid integration, power system operator training system, and cyber-physical transmission and distribution modeling and simulation.